Plant, Cell & Environment

WILEY

Plant, Cell & Environment

ORIGINAL ARTICLE OPEN ACCESS

Carboxylation and Oxygenation Kinetics and Large Subunit (*rbcL*) DNA Sequences for Rubisco From Two Ecotypes of *Plantago lanceolata* L. That Are Native to Sites Differing in Atmospheric CO_2 Levels

Xiaoxiao Shi | Nathan M. Hannon | Arnold J. Bloom

Department of Plant Sciences, University of California at Davis, Davis, California, USA

Correspondence: Arnold J. Bloom (ajbloom@ucdavis.edu)

Received: 28 September 2024 | **Revised:** 10 December 2024 | **Accepted:** 11 December 2024

Funding: National Science Foundation grant CHE-19-04535 funded a portion of this research.

Keywords: adaptation to CO_2-enriched environments | magnesium versus manganese | *Plantago lanceolata* | *rbcL* DNA sequences | rubisco kinetics | specificity for CO_2 over O_2

ABSTRACT

Rubisco, the most prevalent protein on Earth, catalysers both a reaction that initiates C_3 carbon fixation, and a reaction that initiates photorespiration, which stimulates protein synthesis. Regulation of the balance between these reactions under atmospheric CO_2 fluctuations remains poorly understood. We have hypothesised that vascular plants maintain organic carbon-to-nitrogen homoeostasis by adjusting the relative activities of magnesium and manganese in chloroplasts to balance carbon fixation and nitrate assimilation rates. The following examined the influence of magnesium and manganese on carboxylation and oxygenation for rubisco purified from two ecotypes of *Plantago lanceolata* L.: one adapted to the elevated CO_2 atmospheres that occur near a natural CO_2 spring and the other adapted to more typical CO_2 atmospheres that occur nearby. The plastid DNA coding for the large unit of rubisco was similar in both ecotypes. The kinetics of rubiscos from the two ecotypes differed more when associated with manganese than magnesium. Specificity for CO_2 over O_2 ($S_{c/o}$) for rubisco from both ecotypes was higher when the enzymes were bound to magnesium than manganese. Differences in the responses of rubisco from *P. lanceolata* to the metals may account for the adaptation of this species to different CO_2 environments.

1 | Introduction

Central to plant responses to rising atmospheric CO_2 is rubisco (ribulose-1,5-bisphosphate carboxylase-oxygenase), the enzyme that constitutes 50% of the protein in a leaf, 20% of the protein on Earth, and 3% of the global biomass (Bar-On and Milo 2019; Ellis 1979). Rubisco catalyzes several competing reactions (Shi and Bloom 2021). One reaction is the carboxylation of ribulose 1,5-bisphosphate (RuBP) to two molecules of 3-phosphoglyceric acid (3PGA) that initiates C_3 carbon fixation (i.e., Calvin-Benson-Bassham cycle). Rubisco also catalyzes another reaction that generates pyruvate (Andrews and Kane 1991; Shi, Hannon, and Bloom 2024). Finally, rubisco catalyzes a third reaction in which oxygenation of RuBP to one molecule of 3PGA and one molecule of 2PG initiates photorespiration, a process generally considered to dissipate more than 25% of the energy in C_3 plants as waste heat (Smith et al. 2024; South et al. 2019). Photorespiration, however, enhances assimilation of nitrate (NO_3^-) and sulphate (SO_4^-) into amino acids in plant shoots (Abadie and Tcherkez 2019; Bloom 2015a, 2015b, 2019; Bloom et al. 2010; J. Bloom et al. 2014; Bloom and Kameritsch 2017; Bloom, Kasemsap, and Rubio-Asensio 2020; Bloom and

Lancaster 2018; Bloom and Plant 2021; Bloom et al. 2012; Bloom et al. 2002; Carlisle et al. 2012; Dietterich et al. 2015; Easlon and Bloom 2013; Foyer et al. 2009; Myers et al. 2014; Rachmilevitch, Cousins, and Bloom 2004; Rubio-Asensio and Bloom 2017; Asensio, Rachmilevitch, and Bloom 2015; Smart and Bloom 2001; Smart et al. 1998). Therefore, plant protein concentrations decline when elevated CO_2 atmospheres inhibit photorespiration for long periods (Bloom 2015a; J. Bloom et al. 2014; Bloom and Plant 2021; Myers et al. 2014).

A handful of studies conducted more than four decades ago indicated that binding rubisco to Mn^{2+} instead of Mg^{2+} inhibits RuBP carboxylation and accelerates RuBP oxygenation, but the kinetic values were highly variable (Christeller 1981; Christeller and Laing 1979; Jordan and Ogren 1983; Martin and Tabita 1981; Wildner and Henkel 1979). These studies purified rubisco via ammonium sulphate precipitation followed by centrifugation, a protocol that can adversely influence enzyme structure and activation (Iñiguez et al. 2021; Wingfield 1998). In a recent study (Shi, Hannon, and Bloom 2024) that used fast protein liquid chromatography to purify rubisco from five model C_3 species while preserving the metal-binding characteristics of the native protein (Barnett, Scanlan, and Blindauer 2012; Hagège, Huynh, and Hébrant 2015; Montes-Bayón, Blanco-González, and Michalke 2016) and new methods to assess rubisco carboxylation and oxygenation that are indifferent to the presence of Mg^{2+} or Mn^{2+} (Shi, Hannon, and Bloom 2024), the maximum velocity of carboxylation (V_{cmax}) was faster and the Michaelis constant of rubisco for CO_2 (K_c) was greater when rubisco was bound to Mg^{2+} rather than Mn^{2+} (i.e., rubisco had a lower affinity for CO_2 when bound to Mg^{2+} rather than Mn^{2+}). Both $S_{c/o}$ (rubisco specificity for CO_2 over O_2) and V_{cmax}/V_{omax} were greater when the enzyme was bound to Mg^2 rather than Mn^{2+} (Shi, Hannon, and Bloom 2024).

Plantago lanceolata L. may not be a model plant species, but its leaves have been widely used in herbal medicines (Drava et al. 2019; Gonçalves and Romano 2016; Wichtl 2004) and food preparations (Guarrera and Savo 2016). Root fractions of *P. lanceolata* L. possess antibacterial properties (Rahamouz-Haghighi et al. 2022). *P. lanceolata* leaf extracts selectively inhibit the proliferation of CAL51 triple-negative breast cancer cell proliferation (Alsaraf et al. 2019) and have antiobesity effects on mice in vivo (Yoshida et al. 2013). Several flavonoids in the inflorescences and leaves of *P. lanceolata* have anti-allergic and anti-inflammatory effects (Budzianowska and Budzianowski 2022; Murai, Tamayama, and Nishibe 1995).

The following study compared the kinetics of rubisco purified from two ecotypes of *Plantago lanceolata* L.: one ecotype, collected near a CO_2 spring, experienced an average daytime concentration of 791 ppm CO_2 for many generations; the other ecotype, collected 200 m from the spring, experienced ambient CO_2 concentrations of about 421 ppm (Saban, Chapman, and Taylor 2019; Saban et al. 2020; Watson-Lazowski et al. 2016). We also extracted plastid DNA from the two *P. lanceolata* ecotypes and compared the sequences for the large subunit of rubisco (*rbcL*) to determine if multigenerational exposures to different atmospheric CO_2 levels might result in genetic adaptations in rubisco.

2 | Materials and Methods

2.1 | Plant Growth Conditions

Prof. G. Taylor provided us with seeds of *Plantago lanceolata* L. collected in May 2008 from nine plants growing in naturally elevated CO_2 atmospheres near a CO_2 spring at Bossoleto, Italy (Lat. 43°17′, Long. 11°35′) and at a nearby (ca. 200 m apart) ambient CO_2 control site (Saban et al. 2020). Seeds obtained from the two sites were grown for one generation in the glasshouse at the University of Southampton and crossed within maternal families to standardise parental effects. At the University of California at Davis, we planted the two ecotypes into 5 × 5 cm containers containing Sunshine Mix 4 (Sungro, Agawam, MA). Both ecotypes grew in controlled environmental chambers for 21 days at 60% relative humidity (light/dark), air temperature 25°/18°C (light/dark), 16 h of 500 μmol m^{-2} s^{-1} PPFD at canopy height, and atmospheres containing either 450 ppm or 750 ppm CO_2. From both ecotypes, young and mature leaves with similar sizes and growth stages were selected for rubisco extraction.

2.2 | Rubisco Extraction and Purification

We collected about 40 g of leaves and froze them in liquid N_2. Manual grinding with a mortar and pestle lysed the plant cells to a fine powder. We extracted the fine powder in 100 mL of a buffer (50 mM Tris-HCl pH 7.4, 20 mM $MgCl_2$, 20 mM $NaHCO_3$, 0.1 mM Na_2EDTA, 10% glycerol, 50 mM mercaptoethanol, and 1 mM PMSF), filtered the extract through four layers of Miracloth, centrifuged it at 12100 × *g* at 4°C for 15 min to clarify it, and passed the supernatant through a 0.22 μm syringe filter before loading it onto an FPLC column.

We purified rubisco using an ENrich SEC (Size Exclusion Column) 650 10 × 300 Column (BioRad, Hercules, CA) followed by a HiScale 16/20 6 mL SOURCE 30Q column (GE Healthcare Life Sciences, Pittsburgh, PA) on a NGC FPLC system (BioRad, Hercules, CA). All buffers included 2 mM dithiothreitol to prevent intermolecular disulphide bond formation. Pre-equilibration of the size exclusion column involved eluting five column volumes (CV) of 85% buffer A (50 mM Tris-HCl, 1 mM EDTA, 0.1 mM PMSF, pH 7.4) and 15% buffer B (50 mM Tris-HCl, 1 M NaCl 1 mM EDTA, 0.1 mM PMSF, pH 7.4). We loaded the protein sample onto the column and eluted it with 2 CV of 15% buffer B. UV absorption at 280 nm confirmed the protein peak. We (*a*) concentrated the protein solution to around 1 mM, (*b*) exchanged the buffer into buffer A, (*c*) filtered the sample, (*d*) loaded it onto a SOURCE 30Q column pre-equilibrated with 5 CV of buffer A, (*e*) eluted the protein with 50% buffer B with a linear gradient over 10 CV, (*f*) pooled the protein peak at 280 nm, (*g*) exchanged the buffer into buffer A with the addition of 20% glycerol, (*h*) and stored the protein solution at −80°C. We checked the purity of the protein on SDS-PAGE gels, Western Blots, and an Evolution 201 UV/Vis spectrometer coupled with an Evolution 1-cell Peltier temperature control system (Thermo Fisher Scientific, Waltham, MA).

2.3 | Rubisco Carboxylation Colorimetric Reaction

We developed a colorimetric assay for rubisco carboxylation that is accurate in the presence of Mg^{2+} or Mn^{2+} (Shi, Hannon, and Bloom 2024):

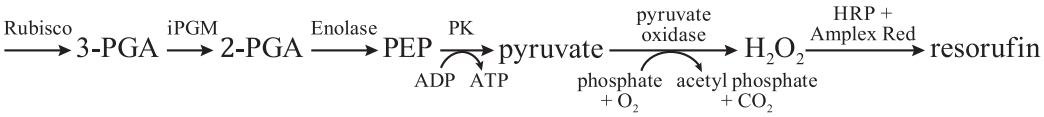

To estimate v_c and V_{cmax}, we assessed the production of 3-PGA in the presence of high levels of CO_2 by iPGM (cofactor-Independent PhosphoGlycerate Mutase) conversion of 3-PGA to 2-PGA (Raverdy et al. 2007; Zhang et al. 2004), followed by a commercial assay kit (2-phosphoglycerate Assay kit, Abcam ab174097) that converts 2-PGA into PEP, then pyruvate, H_2O_2, and resorufin. Absorption at 570 nm monitored resorufin production. This assay can detect 2-PGA levels below 20 pmol and works in the presence of either Mg^{2+} or Mn^{2+}.

In more detail, we activated rubisco before the assays as follows. We added an assay buffer containing 20 mM Tris-HCl, 1 mM EDTA, 100 mM Triethanolamine at pH 7.8 to one 5 mL tube; added 1 or 2 μL of rubisco (0.5–1 μM), 10 μL of 250 mM $NaHCO_3$, 0.5 μL carbonic anhydrase (~2.5 units), and 4 μL of $MgCl_2$ (final concentration 20 mM) or $MnCl_2$ (5 mM), to a total volume of 170 μL; mixed thoroughly; and allowed the mixture to sit for 5 min to allow Rubisco to activate in the presence of a high concentration of CO_2. We sparged the mixture for 1 min with a gas mixture corresponding to the experiment's condition, added 15 μL of iPGM (10 μM), and started the reaction by adding 45 μL of 10 mM RuBP to the tube. To measure the reaction over time, we split the mixture into five tubes and stopped the reaction after 1, 2, 3, 4, or 5 min by adding 0.5 N HCl to each tube. We added KOH to each reaction tube to adjust the pH to about pH 7.8 and added equal amounts of freshly mixed 2-PGA colorimetric cocktail that we prepared from a 2-phosphoglycerate assay kit (ab174097, Abcam, Cambridge, MA), mixed the tubes thoroughly, and moved them to an opaque box to allow the colorimetric cocktail to react without light interference. We measured the OD_{570nm} of each tube after 40 min and calculated the 2-PGA concentration based on a calibration curve determined by adding specific quantities of a 1 mM 2-PGA standard solution that the assay kit provided.

The carboxylation turnover rate $v_c = ½$ (resorufin production rate $- v_o$), where O_2 optode measurements of O_2 depletion estimated v_o as detailed below.

We estimated V_{cmax} from the Michaelis–Menten equation:

$$v_c = \frac{[CO_2] \bullet V_{cmax}}{[CO_2] + K_c(1 + [O_2]/K_o)}$$

and the relative specificity $S_{c/o}$ from:

$$S_{c/o} = \frac{V_{cmax} K_o}{V_{omax} K_c}.$$

We conducted separate calibration runs in the presence of the buffer and Mg^{2+} or Mn^{2+} in the same concentrations used in the rubisco reactions (Supporting Information S1: Figure S1) and calculated the ratio between the slopes of the runs using only the 2-PGA buffer and the slopes of the runs containing rubisco. Linear regressions for each combination of ecotype and metal ion, which included a constant term for each run, expressed the change in 2PGA as a function of time.

2.4 | IPGM Expression and Purification

We transformed a 6 × His-tagged *C. elegans* nematode iPGM plasmid into BL21(DE3) competent cells and incubated them at 37°C overnight. We selected one colony for culturing at 37°C overnight in 50 mL LB media (peptone 10 g, yeast extract 5 g, NaCl 10 g L^{-1}) and 50 μL 100 g mL^{-1} kanamycin stock solution. We added 10 mL of the small culture to 1 L of the same media and grew it until OD_{600} = 0.7. We added isopropyl β-D-1-thiogalactopyranoside (IPTG) to the culture flask to bring it to a final concentration of 0.2 mM and reduced the temperature and stirring speed to 30°C and 100 rpm, respectively. We grew the culture for 24 h, centrifuged it for 20 min at 4700 × *g*, and suspended the pellet in 30 mL buffer A (20 mM Tris-HCl, 2 mM DTT, pH 6.8). We stored the cell suspension at −80°C before purification.

We thawed 30 mL of the cell suspension, lysed the cells by adding 30 mg of lysozyme and 30 μg of DNAse, and passed the cells twice through a French press. We centrifuged the solution at 120100 × *g* for 60 min, concentrated the supernatant using Amicon Ultra Centrifuge Filters (EMD Millipore, Burlington, MA), and filtered the resulting solution through a 0.22 μm filter before loading it onto a column.

We pre-equilibrated a Bio-Scale Mini Profinity IMAC cartridge (Bio-Rad, Hercules, CA) with five column volumes (CV) of buffer A (50 mM Tris-HCl, 25 mM imidazole, 1 mM EDTA, 0.1 mM PMSF, pH 7.4), loaded the protein sample onto the column, washed the column with 5 CV of buffer A, and eluted the protein with a linear gradient over 10 CV of buffer B (50 mM Tris-HCl, 500 mM imidazole, 1 mM EDTA, 0.1 mM PMSF, pH 7.4), confirmed the protein peak by UV absorption at 280 nm, and loaded the fractions onto an SDS-PAGE gel. We stored the fractions with iPGM protein at −80°C.

2.5 | Rubisco Oxygenation

A needle-type micro-optode OXF50-OI (PyroScience GmbH, Breman, Germany) on a FireSting O_2 optical oxygen and

temperature metre (FSO2-4) monitored changes in dissolved O_2 concentration. We conducted oxygenation experiments under four sets of conditions at 25°C: (*a*) ambient (79% N_2, 20.96% O_2, and 0.04% CO_2), (*b*) elevated CO_2 (78.96% N_2, 20.96% O_2, and 0.08% CO_2), (*c*) reduced O_2 (89% N_2, 10.96% O_2, and 0.04% CO_2), and (*d*) elevated O_2 (69.96% N_2, 30% O_2, and 0.04% CO_2. Precision mass flow controllers (Apex Vacuum, Canton, GA) calibrated against soap bubble flowmeters mixed pure N_2, O_2, and CO_2 to the desired concentrations. A nondispersive Infra-red Gas Analyser (Li-cor, Lincoln, NE) checked the CO_2 concentration. We conducted a two-point calibration of the oxygen optode in both air and air-saturated water. Air-saturated water was obtained by vigorously shaking a covered glass beaker half full of deionized water for 1 min, and the calibration was performed using the optode's software with the needle immersed in air or air-saturated water. The final assay volume in each tube was 3000 μL.

Before the oxygenation assay, we activated rubisco as follows. We added assay buffer (20 mM Tris-HCl, 1 mM EDTA, 10 mM $NaHCO_3$, 100 mM triethanolamine, pH 7.8) to a covered, temperature-controlled, 4 mL quartz cuvette; added 10 μL of rubisco (0.5–1 μM), 5 μL carbonic anhydrase (~25 units), and 40 μL of $MgCl_2$ (final concentration 20 mM) or $MnCl_2$ (5 mM) to a total volume of 300 μL. We mixed the contents of the cuvette thoroughly and allowed the mixture to sit for 5 min to activate rubisco. We added additional buffer to bring the total volume to 2910 μL before inserting the oxygen sensor and sparging for 1 min with the gas mixture corresponding to the experiment's conditions. After about 30 s, once the oxygen sensor reading stabilised, we started the reaction by adding 90 μL of 10 mM RuBP (pre-equilibrated with the same gas mixture) and began collecting data. In all experiments, we observed that the decrease in oxygen levels was linear over 300 s or more, as opposed to the exponential curve that would be expected if there were significant protein deactivation and degradation over this time. Therefore, we estimated the oxygenation turnover rate v_o from the linear trend in oxygen consumption for at least 200 s divided by rubisco content.

Michaelis–Menten kinetics predicts the oxygenation turnover rate v_o to be:

$$v_o = \frac{[O_2] \bullet V_{omax}}{[O_2] + K_o(1 + [CO_2]/K_c)},$$

where V_{omax}, K_o, and K_c depend on species and the associated metal, Mn^{2+} or Mg^{2+}, but are independent of $[O_2]$ and $[CO_2]$. Values of v_o under multiple sets of conditions for $[O_2]$ and $[CO_2]$, therefore, provided estimates of the three parameters V_{omax}, K_o, and K_c. For the elevated O_2 experiments, we performed blank runs with RuBP and all other components but without rubisco. We calculated O_2 consumption rates before and after adding RuBP for both the blank and actual runs and determined the O_2 consumption rate from

$$O_2 consumption = R_{rubisco,RuBP} - R_{rubisco} - (R_{RuBP} - R_{neither}),$$

where R denotes the rate of change in oxygen levels in the presence or absence of rubisco and RuBP.

2.6 | Statistics

In general, we used R for Windows version v.4.3.3 and will provide the R code upon request. In performing experiments, we prioritised additional replicates of conditions that would reduce the variance of our estimates. From the measured rates of rubisco reactions, kinetic parameters were calculated using a Bayesian method. This method did not use response curves in the traditional way but rather calculated the most likely values of kinetic parameters based on experiments performed under four sets of conditions as well as existing knowledge of Rubisco kinetics. Briefly, a lognormal prior distribution for each of the kinetic parameters V_{cmax}, V_{omax}, k_c, and k_o was centred around 2.95 s^{-1}, 0.9 s^{-1}, 10.5 μM, and 311 μM, respectively, with a logarithmic standard deviation of 0.4. These were chosen based on published values of kinetic parameters for C_3 plants, with a variance chosen to favour values similar to published values but still allow for the possibility that *Plantago lanceolata* has different properties. From this prior distribution, multiple sets of kinetic parameters were chosen at random and the relative likelihood of observing the values in our experiments was computed for each set of kinetic parameters. The result of each experiment was assumed to be normally distributed with a fixed variance, combining the regression standard error in the measurements with the variance among the results of similar experiments. These likelihoods were used as weights to approximate a posterior distribution on the kinetic parameters from which we calculated posterior means and standard deviations of each parameter. To determine the overall effects of Mg^{2+} and Mn^{2+} across the two ecotypes, we aggregated each kinetic parameter, adjusted by their respective standard errors, and used it as input to a two-way ANOVA, with metal ion and ecotype as variables.

2.7 | *rbcL* Sequences

We isolated chloroplasts (Bloom and Kameritsch 2017) from the two *P. lanceolata* ecotypes and extracted the plastid DNAs using the modified high salt method (Shi et al. 2012). A_{260}/A_{280} ratios were verified by UV-Vis spectrophotometry, and samples with a ratio over 2 were sent for chloroplast genomic DNA sequencing (CD Genomics, Shirley, NY). After conducting the initial sample quality test, high-quality DNA samples were used to construct the library. The purified DNA samples were fragmented into 200-500 bp using a Covaris S/E210 or Bioruptor. The overhangs resulting from the fragmentation were converted into blunt ends using T4 DNA polymerase, Klenow Fragment, and T4 Polynucleotide Kinase. Subsequently, an 'A' base was added to the 3′ end of the blunt phosphorylated DNA fragments, followed by the ligation of adaptors to the ends of the DNA fragments. The desired fragments were then purified through gel-electrophoresis, selectively enriched, and amplified by PCR. Index tags were introduced into the adaptor during the PCR stage, and a library quality test was performed. Finally, the qualified library was used for sequencing using Illumina PE150 Sequencing Platform, and the generated data were utilised for downstream bioinformatics

analysis. GetOrganelle (v1.7.7.1) was used to construct the final cpDNA sequences. Custom R code (v4.3.3) was used to search for fragments containing variants of the cpDNA sequences and determine their frequencies. For each identified variant, a sequence of five codons centered on the changed nucleotide(s) was chosen, and the number of fragments containing the original and variant sequences was compared to calculate its frequency in both ecotypes.

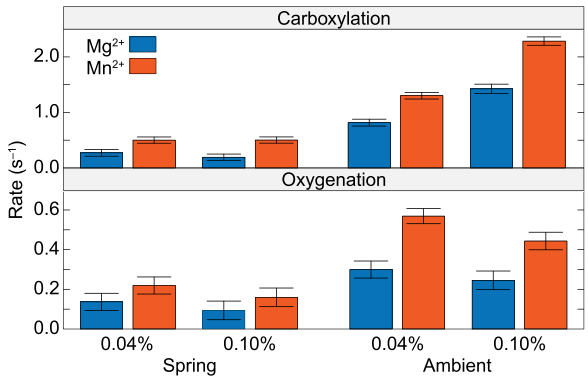

FIGURE 1 | Rates of RuBP carboxylation and oxygenation in turnovers per second by rubisco purified from two ecotypes of *Plantago lanceolata* L. One ecotype (Spring) collected near a CO_2 spring had experienced high CO_2 for many generations, and the other ecotype collected nearby (Ambient) had experienced ambient CO_2 atmospheres. The enzyme was bound to Mg^{2+} or Mn^{2+} and exposed to 21% O_2 and 0.04% or 0.10% CO_2. Shown are the mean ± SE, $n = 4–10$. [Color figure can be viewed at wileyonlinelibrary.com]

3 | Results

3.1 | Rubisco Kinetics

Rubisco purified from the ambient ecotype conducted both RuBP carboxylation and oxygenation at higher rates under all conditions than rubisco purified from the CO_2-spring ecotype (Figures 1 and 2). Rubisco from the ambient ecotype conducted significantly faster carboxylation under 0.10% CO_2 than 0.04% CO_2, whereas rubisco from the spring ecotype was much less affected by CO_2 enrichment (Figure 1 and 2). When bound to Mn^{2+}, rubisco from the ambient ecotype conducted significantly faster RuBP carboxylation under high CO_2 and ambient conditions, and significantly faster oxygenation under ambient conditions than when bound to Mg^{2+}. Rubisco from the spring ecotype conducted significantly faster carboxylation under high CO_2 conditions when bound to Mn^{2+} than when bound to Mg^{2+} (Figure 2).

The kinetics of the rubiscos from the two ecotypes differed more when they were associated with Mn^{2+} than Mg^{2+}(Figure 3). The rubisco from the ambient ecotype exhibited slightly higher V_{cmax} and V_{omax} than the rubisco from the spring ecotype when bound to Mg^{2+} and much higher V_{cmax} and V_{omax} when bound to Mn^{2+} (Figure 3). Specificity for CO_2 over O_2 ($S_{c/o}$) for rubiscos from both ecotypes were higher when the enzymes were bound to Mg^{2+} than Mn^{2+} (Figure 3).

Although measurements of physiological characteristics are beyond the scope of the current study, visual inspection revealed distinct physiological differences between the two ecotypes, including a larger average seed size and lower seed

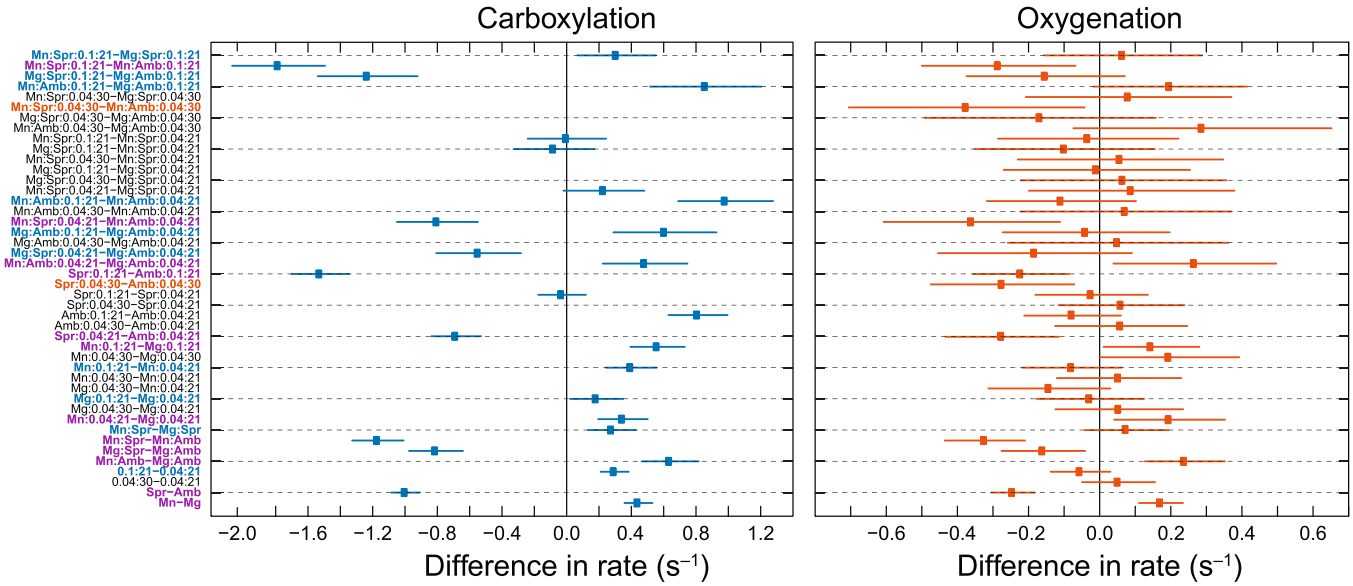

FIGURE 2 | Tukey test comparing RuBP carboxylation and oxygenation rates under various combinations of metals (Mg^{2+} vs. Mn^{2+}), *Plantago lanceolata* ecotypes (Spr vs. Amb), CO_2 concentrations (0.04% vs. 0.1%), and O_2 concentrations (21% vs. 30%). Shown are mean difference ± SE, $n = 4–10$. Labels in blue designate that only carboxylation differed, labels in red designate that only oxygenation differed, labels in purple designate that both carboxylation and oxygenation differed, and labels in black designate that neither carboxylation nor oxygenation differed. For example, in the top line, carboxylation of the Mn^{2+}-treated rubisco from the Spring ecotype tested at 0.1% CO_2 and 21% O_2 was greater than carboxylation of the Mg^{2+}-treated rubisco, but oxygenation did not differ significantly. For additional statistical analyses, see Supporting Information S1: Tables S1 and S2. [Color figure can be viewed at wileyonlinelibrary.com]

yield per flower and per plant in the CO_2-spring ecotype (data not shown). Our observations on various average physiological characteristics of several spring and ambient ecotypes of *Plantago lanceolata* indicated that these differences did not affect the plants' overall fitness and growth; therefore we concluded that these changes were likely genotype-specific and could not be explained by CO_2 conditions alone.

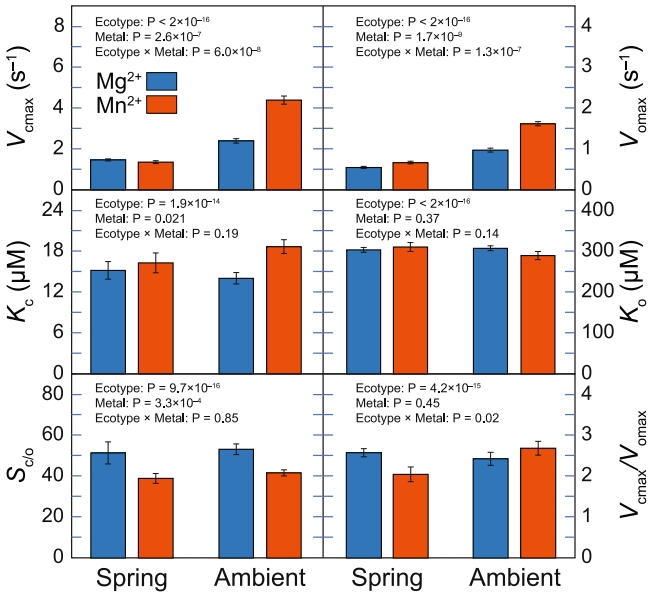

FIGURE 3 | Influence of Mg^{2+} or Mn^{2+} (mean ± credible interval, $n = 4–20$) on the kinetics of rubisco purified from two ecotypes of *Plantago lanceolata* L.: one (Spring) collected near a CO_2 spring has experienced high CO_2 for many generations; the other collected nearby (Ambient) has experienced ambient CO_2. V_{cmax} is the maximum velocity of carboxylation, V_{omax} is the maximum velocity of oxygenation, K_c is the Michaelis constant of rubisco for CO_2, K_o is the Michaelis constant of rubisco for O_2, $S_{c/o}$ is the specificity of rubisco for CO_2 over O_2, and V_{cmax}/V_{omax} is the ratio of the maximum velocities. Also displayed are the 2-way ANOVAs for the influence of Ecotype, Metal, or their interaction on the kinetic parameters for rubiscos purified from the two ecotypes in the presence of Mg^{2+} or Mn^{2+}. For additional statistical analysis, see Supporting Information S1: Table S3. [Color figure can be viewed at wileyonlinelibrary.com]

3.2 | cpDNA Sequences

Both ecotypes had similar plastid DNA coding for the large unit of rubisco (*rbcL*). The *rbcL* gene is located at positions 53249–54682 in the ambient ecotype and 53018 to 54451 in the elevated ecotype of the chloroplast DNA sequences (cpDNAs). Gene maps showing the *rbcL* encoding regions and the translation directions are displayed in Figure 4. The *rbcL* gene in the reconstructed sequences was identical to those in previously published sequences (Saban et al. 2020; Zhao et al. 2023). A small percentage of the fragments, however, differed from this sequence in one or, in one case, two nucleotides (Table 1). The most common of these differences was a change in nucleotide 890 from A to C, which occurred in approximately 5.6% of fragments in the spring ecotype and 4.1% in the ambient. This change replaces the methionine at residue 297 with a leucine.

4 | Discussion

4.1 | Kinetics

The ambient ecotype had overall higher rates of both carboxylation and oxygenation than the CO_2-spring ecotype. Although *Plantago lanceolata* exhibits changes in growth habit and phenology under different growth conditions; genetic variation is responsible for significantly different seed yields on the original and alien sites (Tienderen and van der Toorn 1991). Under limited water supply and high light exposure, *P. lanceolata* displayed higher water use efficiency (WUE), better nitrogen absorption, and higher bacterial frequency in roots (Miszalski et al. 2023). The photochemical activity of PSII was similar under stressed and benign conditions (Miszalski et al. 2023).

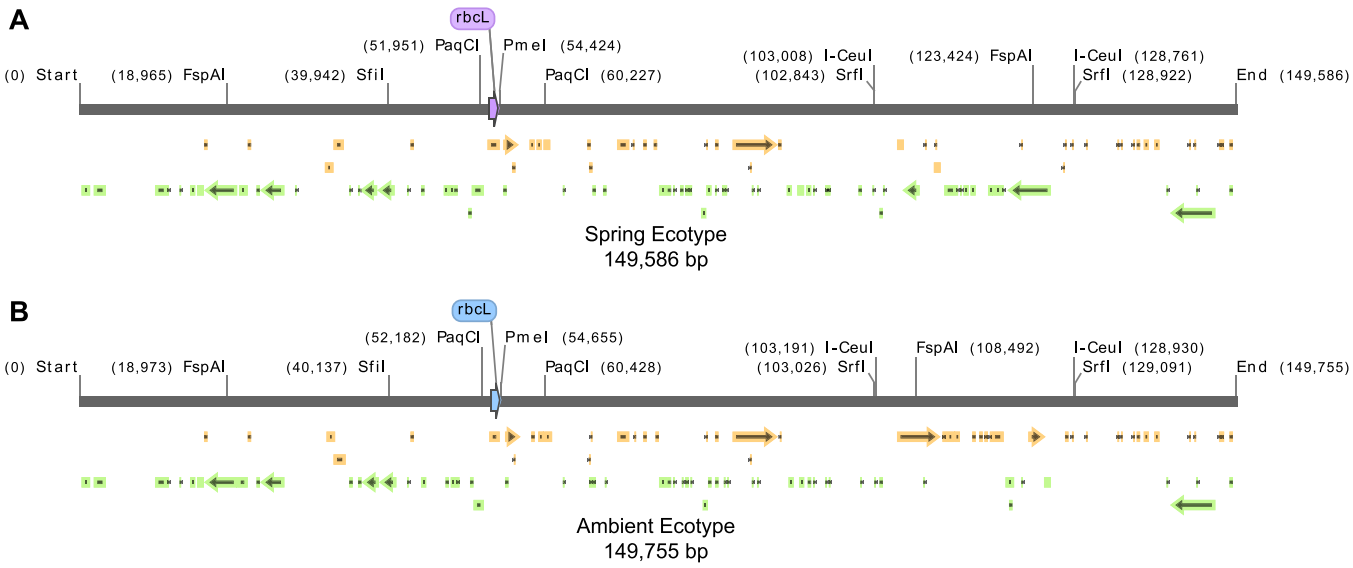

FIGURE 4 | cpDNA map of *rbcL* from the (A) CO_2-spring and (B) ambient ecotypes. The orange and green arrows indicate open reading frames (ORFs). The restriction enzymes shown are unique and dual cutters. [Color figure can be viewed at wileyonlinelibrary.com]

TABLE 1 | Mutations that appeared in a significant portion of the fragments matching the *rbcL* gene in two ecotypes of *Plantago lanceolata*. "Positions" refer to the positions of the changed nucleotide (s) and are specified relative to the start of the *rbcL* gene. "Frequency" refers to the number of fragments containing the changed sequence as a percentage of the total number of fragments containing the original sequence and the changed sequence.

Position(s)	Original DNA	Changed DNA	Original translated amino acid sequence	Changed translated amino acid sequence	Frequency in CO_2-spring ecotype	Frequency in ambient ecotype
842	AGCTTGGCTCATTAT	AGCTTGCCTCATTAT	SLAHY	SLPHY	0.04%	0.47%
890	CGTGCAATGCATGCA	CGTGCACTGCATGCA	RAMHA	RALHA	5.57%	4.14%
913, 918	AGACAGAAGAATCAT	AGACAAAAGACTCAT	RQKNH	RQKTH	0.00%	1.30%
936	CACTTCCGTGTACTA	CACTTCCATGTACTA	HFRVL	HFHVL	0.16%	1.60%
1012	CTGGAAGGAGAAAGA	CTGGAAGGGGAAAGA	LEGER	LEGER	0.04%	1.16%
1153	ATTCACGTTTGGCAT	ATTCACGTCTGGCAT	IHVWH	IHVWH	0.00%	1.25%
1161	TGGCATATGCCTGCT	TGGCATACGCCTGCT	WHMPA	WHTPA	0.05%	1.63%
1196	GATTCCGTACTACAG	GATTCCATACTACAG	DSVLQ	DSILQ	0.26%	0.94%
1389	GTATGGAAAGAGATC	GTATGGACAGAGATC	VWKEI	VWTEI	1.43%	1.57%

The CO_2-spring ecotype showed weak selection in exons compared to the ambient ecotype in a study of a wild *Plantago* population's response to multigenerational exposure to elevated atmospheric CO_2 (Saban et al. 2020). Overall genetic differentiation was low, but some differential methylation occurred after single generation of exposure to elevated CO_2, and significant differentiation occurred after multiple generations between the CO_2-spring ecotype and CO_2 ambient ecotype in a methylome analysis (Saban et al. 2020). Differential expression (DE), differential methylation, and single nucleotide polymorphisms may influence adaptation to elevated CO_2 (Saban et al. 2020). In 59 transcripts, genes responsible for nitrogen use efficiency (NUE) and stomatal patterning were coded, and DE genes and sites of differential methylation or single nucleotide polymorphisms were co-located (Saban et al. 2020). Taken together, we think the extensive plasticity of *P. lanceolata* might be shared among many species from various geographic locations, and the variations in photosynthetic rates are genotype-specific. The possible differences in genomic DNA and corresponding adaptations to elevated CO_2 conditions warrant additional study.

Exposure to elevated CO_2 atmospheres stimulated carboxylation rates in the ambient ecotype more than in the CO_2-spring ecotype. This would not be expected if faster carboxylation rates were always beneficial. If balancing carboxylation and oxygenation is advantageous, then elevated and, especially, fluctuating levels of CO_2 might select for a mechanism where carboxylation became less sensitive to atmospheric CO_2. The nature of such a mechanism is unknown. The CO_2-spring ecotype has adapted to elevated CO_2 levels for many generations and might be expected to balance carboxylation and oxygenation more quickly, and the observed response of the spring ecotype to higher CO_2 is consistent with it doing so.

Note that the 0.1% CO_2 treatment used in this study is generally insufficient to saturate rubisco carboxylation, so the lack of significant change in the CO_2-spring ecotype between ambient and 0.1% CO_2 conditions may indicate an additional regulatory mechanism beyond the usual kinetics. The change from methionine at residue 297 with leucine is too rare to have a significant effect on the overall kinetics. Possibly, the gene for the small subunit of rubisco *RbcS* or other nuclear-encoded genes, had some regulatory effect, perhaps by altering the conformation of the large subunit when exposed to elevated CO_2. Rubisco is also known to be subject to posttranslational modifications (Houtz, Magnani, Nayak, & Dirk. 2008), and additional studies will be necessary to understand if these have a regulatory effect.

The kinetics of rubisco from *P. lanceolata* differed in several ways from those of other C_3 plants (Shi, Hannon, and Bloom 2024). Both the ambient and CO_2-spring ecotypes had a higher K_c compared to *Arabidopsis*, rice, wheat, spinach, and tobacco, and a lower V_{omax} compared to *Arabidopsis*, wheat, and spinach. Furthermore, the response to Mn^{2+} of rubisco from *P. lanceolata*—particularly the ambient ecotype—differed from that of other C_3 plants. In other species, carboxylation rates were higher when rubisco was bound to Mg^{2+}, whereas oxygenation rates were higher when bound to Mn^{2+} (Shi, Hannon, and Bloom 2024). By contrast, Mn^{2+} appears to accelerate both carboxylation and oxygenation in rubisco from

Plantago lanceolata. In previous studies (Bloom and Kameritsch 2017), plants responded to higher levels of CO_2 by increasing Mn^{2+} levels. If rubisco from *P. lanceolata* performs faster carboxylation and oxygenation in the presence of Mn^{2+} than that from other plants, this may explain why this species was successful in the high CO_2 environment of the spring. Additional studies will be needed to determine why rubisco from *P. lanceolata* functions this way and if other species behave similarly.

In vitro experiments on photosynthetic carbon fixation and photorespiration conducted during the past four decades removed all Mn^{2+} from plastid enzymes and replaced the Mn^{2+} with Mg^{2+} (Bloom and Kameritsch 2017; Bloom and Lancaster 2018; Shi and Bloom 2021). Excluding Mn^{2+} from such experiments seems incongruous with the evolution of oxygenic photosynthesis and the Great Oxidation Event that began 2.3 to 2.5 billion years ago when soluble Mn^{2+} increased near Earth's surface (Fischer, Hemp, and Johnson 2016; Lingappa et al. 2019) and photosynthetic organisms proliferated that had (*a*) an Mn^{2+} complex in photosystem II that split water and released O_2 (Fischer, Hemp, and Johnson 2016; Lingappa et al. 2019), (*b*) Mn^{2+}-containing compounds that provided cellular protection against oxidative stress (Fischer, Hemp, and Johnson 2016; Lingappa et al. 2019), (*c*) a Form I rubisco that had more than one hundred times greater affinity for Mn^{2+} than Mg^{2+} (Bloom and Kameritsch 2017), and (*d*) photorespiratory reactions that accelerated when the enzymes involved are bound to Mn^{2+} instead of Mg^{2+} (Christeller 1981; Christeller and Laing 1979; Hagemann et al. 2016; Jordan and Ogren 1983; Martin and Tabita 1981; Segura-Broncano et al. 2023; Wildner and Henkel 1979).

When bound to Mg^{2+}, kinetic parameters for rubisco from both *Plantago* ecotypes were similar to those from other C_3 plants (Shi, Hannon, and Bloom 2024). Nonetheless, if the CO_2-spring ecotype has a mechanism that preserves the balance of carboxylation and oxygenation under elevated CO_2, as introduced above, then Michaelis–Menten kinetics might not fully characterise it. Under Michaelis–Menten kinetics, $S_{c/o}$, a constant, equals the ratio of carboxylation to oxygenation divided by the ratio of CO_2 to O_2:

$$S_{c/o} = \frac{V_c[O_2]}{V_o[CO_2]}$$

If this quantity is not constant—as might happen if an additional regulatory mechanism functions in the presence of higher levels of CO_2—then Michaelis–Menten kinetics might not be appropriate. In this case, the calculated Michaelis–Menten kinetic parameters might be "best fits" to the data but might underestimate carboxylation and overestimate oxygenation under ambient CO_2, and do the reverse under elevated CO_2.

4.1.1 | Chloroplast DNA Sequences

The reconstructed sequences for *rbcL* from *P. lanceolata* were nearly identical to the previously published sequences for the *rbcL* gene (Saban et al. 2020; Zhao et al. 2023). This is consistent with the generality that the *rbcL* gene is highly conserved among species (Saban et al. 2020) and the *P. lanceolata*-specific findings of low overall genetic differentiation between the CO_2 elevated and ambient ecotypes and weak selection in exons (Saban et al. 2020). Although DNA methylation may play a role in *P. lanceolata*'s evolutionary divergence under exposure to elevated and ambient CO_2 for multiple generations (Saban et al. 2020), we did not conduct cpDNA bisulfite sequencing because chloroplast DNA is relatively insensitive to methylation (Ahlert et al. 2009; Fojtová, Kovařík, and Matyášek 2001) and because in particular *rbcL* genes in tobacco, *Arabidopsis*, peas, and tomatoes are not affected by DNA methylation (Fojtová, Kovařík, and Matyášek 2001). Moreover, the BstNI/EcoRII assay, which had been used in previous studies, might not be accurate for analysing low levels of methylation in chloroplast DNA sequences (Langdale, Taylor, and Nelson 1991; Marano and Carrillo 1991; Ngernprasirtsiri, Kobayashi, and Akazawa 1988; Ohta et al. 1991). Increasing adenine or cytosine methylation by introducing cyanobacterial genes for adenine and cytosine DNA methyltransferases into the tobacco plastid genome through chloroplast transformation resulted in no phenotypic differences with wild-type plants and no alterations in plastid gene expression (Ahlert et al. 2009).

The heteroplastidic variant of the *rbcL* gene with a C, instead of an A, at position 890 occurred in both *P. lanceolata* ecotypes at a much higher frequency than other mutations (Table 1). This DNA change corresponds to a change from Met 297 to Leu 297 in the amino acid sequence, which we might evaluate by examining the related — and well-studied — spinach rubisco sequence. Rubisco crystal structures from spinach show residue 297 in close proximity to the substrate access channel (Figure 5). In an activated transition state analogue that was achieved by binding to the tight-binding inhibitor CAP, Mg^{2+} coordination is in a distorted octahedron with longer than usual metal-R bond distances (Figure 5A) (Andersson 1996). This is the "closed" active site conformation. In another activated structure with the substrate RuBP and Ca^{2+}, residue 297 moves to hover over the active site channel, whereas Lys334, an important residue for turning over rubisco, moves away from the reaction centre (Figure 5B). Note that Ca^{2+} in Figure 5B can activate rubisco but does not enable it to turn over (Karkehabadi, Taylor, and Andersson 2003; Taylor and Andersson 1997). The active site remains in an "open" conformation.

Although interconversions of hydrophobic residues such as those from methionine to leucine are common and enzyme function before and after such changes often remain the same, residue 297 should not be ignored. It is located right at the entrance of the active site and at the end of the flexible part of a loop. Loop movements involving residue 297 might also interact with neighbouring loops such as the loop containing the carbamylated Lys201 that is required for CO_2 activation or the loop on the distal side of the substrate containing Lys334, whose interactions with substrate-CO_2 complex are required for turning rubisco over (Cleland et al. 1998). Lys334 is also believed to stabilise the transition state and the product (Cleland et al. 1998) during the reactions when the active site is in the "closed" conformation (Figure 5A). The distances of the

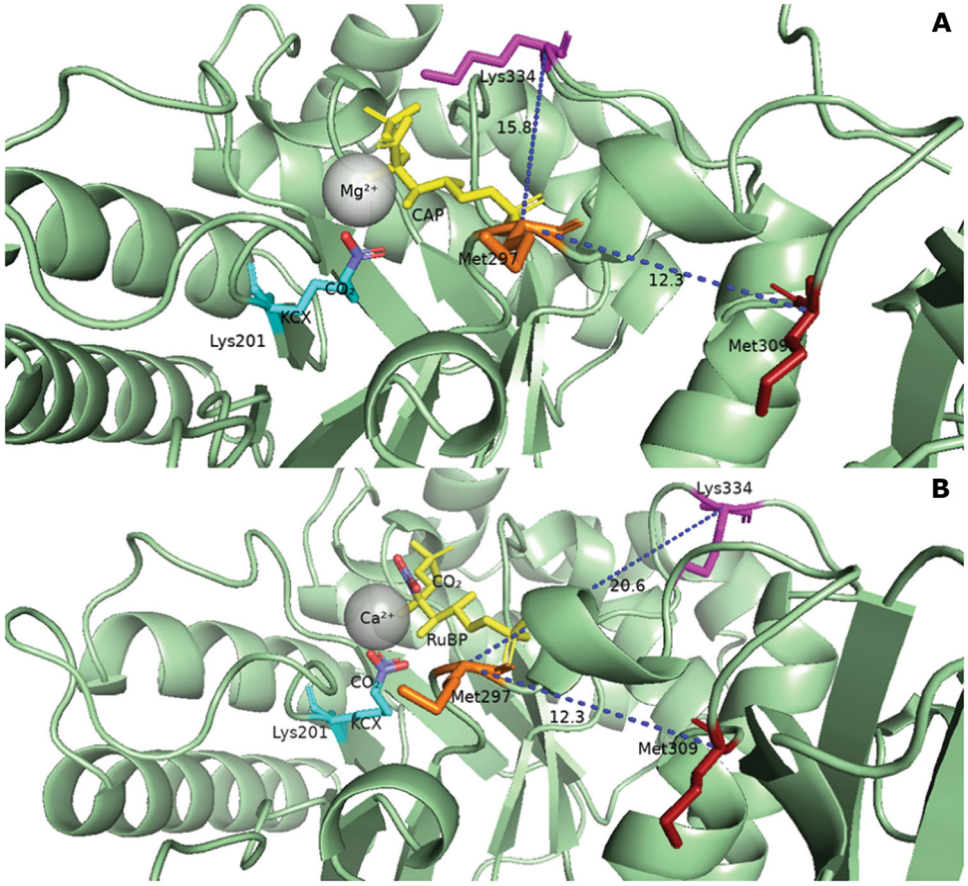

FIGURE 5 | Portions of two published crystal structures of spinach rubisco showing the substrate, metal ion, and nearby residues of interest. (A) Rubisco bound to Mg^{2+} and CAP (PDB: 8RUC) (Andersson 1996). (B) Rubisco bound to Ca^{2+} and RuBP (PDB: 1RXO) (Taylor and Andersson 1997). KCX denotes the catalytic carbamylated lysine and CAP denotes 2-carboxyarabinitol-1,5-diphosphate. [Color figure can be viewed at wileyonlinelibrary.com]

C-alpha in Lys 334 to Met 297 changed from 20.6 Å to 15.8 Å from the open (Figure 5B) to the closed state (Figure 5A). Met309, which is located near the large subunit interface, is believed to be the C_3/C_4 catalytic switch residue (Whitney et al. 2011) and retained its 12.3 Å distance to Met297, regardless of the conformational changes in the open and closed structures. The M297L variant encoded by this version of the gene might have properties that are advantageous under CO_2 enrichment, such as regulating the opening and closing of the active site access tunnel, which might favour this variant in the CO_2-spring ecotype. A high CO_2 environment, thus, might gradually select for a higher percentage of chloroplasts containing this variant, causing the frequency of the variant to increase over time. The current frequency of the variant, however, is insufficient to account for differences between the two ecotypes.

The second most frequent (1.43% for spring and 1.57% for ambient ecotypes) change occurs at position 1389, where residue lysine 463 is mutated into threonine. The residue is located at the beginning of the final loop at the C-terminal of Rubisco. This loop is located on the proximal side of the substrate, but it poses an over 20 Å distance to the substrate based on the published spinach structure. Considering the flexibility of an end-of-translation loop, we do not think this change would account for any functional changes in the enzyme. The subsequent two mutations in line for about 1.7% of both genotypes are position 1161 (residue 387) and 936 (residue 312). Residue 387 is located on a buried helix but directly follows the active-site-interacting loop involving residues 378–384. Residue 312 is on the helix downstream to Met309, which is on the large subunit interface (Whitney et al. 2011).

The type I rubisco large subunit gene (*rbcL*) has evolved slower than 98% of other enzymes (Bouvier, Emms, and Kelly 2024). A phylogenetic study found that one nucleotide substitution and one amino acid change happen every 0.9 million years and 7.2 million years, respectively (Bouvier, Emms, and Kelly 2024). This is consistent with the 4%–5% occurrences of the mutation we observed at position 890 on the *rbcL* gene.

Adaptation of the rubisco protein, which was previously thought to derive from changes in *rbcL* (Kapralov and Filatov 2007), could also be influenced by variations within the gene that encodes the small subunit (Yamada et al. 2019). There are 13 positions along the *rbcS* sequence that show evidence of positive selection and coevolution with the *rbcL* gene (Yamada et al. 2019). The β/α-barrel domains of two *rbcL* subunits have the majority of polar interactions with the *rbcS* N-terminal region (Knight, Andersson, and Brändén 1990). Based on available crystal structures, eukaryotic Rubiscos only bind one *rbcS* isoform per L_8S_8 complex, even though most species have multiple nuclear-encoded *rbcS* isoforms (Mao et al. 2023). Although

rbcS affects the assembly and catalytic performance of the Form I rubisco (Spreitzer 2003), how environmental changes such as increasing CO_2 concentration influence the regulatory pathways of *rbcS* isoform selections and the extent to which different selections/assemblies of the complex alter rubisco kinetics remain unknown. Molecular dynamics simulations on extant and ancestral rubisco sequences showed that the small subunit (*rbcS*) consistently confined the structural dynamics of the large subunit throughout the enzyme's evolutionary history (Amritkar, Cuevas, & Kacar, 2024). The data were inconclusive, however, on whether the small subunit serves as a CO_2 substrate reservoir (Amritkar et al. 2024), as some have proposed (van Lun et al. 2014). This may be because each species contains only one copy of the *rbcL* gene in the chloroplast, whereas multiple *rbcS* sequences are found encoded in genomic DNAs, and *rbcS* evolves faster (Bouvier, Emms, and Kelly 2024). This might also explain the kinetic differences between spring and ambient genotypes, but clearly, additional studies on the function of rubisco small subunit are required.

5 | Conclusions

The kinetic properties of rubisco from *P. lanceolata* generally align with those of other C_3 plant species. Nonetheless, notable differences exist. In *P. lanceolata*, rubisco exhibits faster carboxylation and oxygenation when it is associated with Mn^{2+} than when it is associated with Mg^{2+}. This disparity may account for the ability of this species to acclimate to high CO_2 environments. The *rbcL* gene, which is identical in both ecotypes except for a higher frequency of a rare variant in the spring ecotype, cannot explain differences between the two ecotypes.

Data on rubisco kinetics from non-model plant species remain limited, underscoring the need to examine the factors contributing to the differences between *P. lanceolata* ecotypes and among *P. lanceolata* and model species. Elucidating the role of metals Mn^{2+} versus Mg^{2+} within the photosynthetic and photorespiratory pathways should enhance our understanding of plant adaptations to climate change.

Acknowledgements

NSF grant CHE-19-04535 funded a portion of this research.

Data Availability Statement

Data used in this work have been uploaded to Dryad and will be made public upon publication.

References

Abadie, C., and G. Tcherkez. 2019. "Plant Sulphur Metabolism Is Stimulated by Photorespiration." *Communications Biology* 2, no. 1: 379. https://doi.org/10.1038/s42003-019-0616-y.

Ahlert, D., S. Stegemann, S. Kahlau, S. Ruf, and R. Bock. 2009. "Insensitivity of Chloroplast Gene Expression to DNA Methylation." *Molecular Genetics and Genomics* 282: 17–24.

Alsaraf, K. M., M. H. Mohammad, A. M. Al-Shammari, and I. S. Abbas. 2019. "Selective Cytotoxic Effect of *Plantago Lanceolata* L. Against Breast Cancer Cells." *Journal of the Egyptian National Cancer Institute* 31: 10.

Amritkar, K., B. Cuevas, and B. Kacar. 2024. "Ancestral Structure Prediction Reveals the Conformational Impact of the RuBisCO Small Subunit Across Time." *bioRxiv*: 597628.

Andersson, I. 1996. "Large Structures at High Resolution: The 1.6 Å Crystal Structure of Spinach Ribulose-1, 5-Bisphosphate Carboxylase/Oxygenase Complexed With 2-Carboxyarabinitol Bisphosphate." *Journal of Molecular Biology* 259, no. 1: 160–174.

Andrews, T. J., and H. J. Kane. 1991. "Pyruvate is a By-Product of Catalysis by Ribulosebisphosphate Carboxylase/Oxygenase." *Journal of Biological Chemistry* 266, no. 15: 9447–9452.

Asensio, J. S. R., S. Rachmilevitch, and A. J. Bloom. 2015. "Responses of Arabidopsis and Wheat to Rising CO_2 Depend on Nitrogen Source and Nighttime CO_2 Levels." *Plant Physiology* 168, no. 1: 156–163. https://doi.org/10.1104/pp.15.00110.

Barnett, J. P., D. J. Scanlan, and C. A. Blindauer. 2012. "Protein Fractionation and Detection for Metalloproteomics: Challenges and Approaches." *Analytical and Bioanalytical Chemistry* 402, no. 10: 3311–3322.

Bar-On, Y. M., and R. Milo. 2019. "The Global Mass and Average Rate of Rubisco." *Proceedings of the National Academy of Sciences* 116, no. 10: 4738–4743. https://doi.org/10.1073/pnas.1816654116.

Bloom, A. J. 2015a. "The Increasing Importance of Distinguishing Among Plant Nitrogen Sources." *Current Opinion in Plant Biology* 25: 10–16. https://doi.org/10.1016/j.pbi.2015.03.002.

Bloom, A. J. 2015b. "Photorespiration and Nitrate Assimilation: A Major Intersection Between Plant Carbon and Nitrogen." *Photosynthesis Research* 123, no. 2: 117–128. https://doi.org/10.1007/s11120-014-0056-y.

Bloom, A. J. 2019. "Metal Regulation of Metabolism." *Current Opinion in Chemical Biology* 49: 33–38.

Bloom, A. J., J. S. R. Asensio, L. Randall, S. Rachmilevitch, A. B. Cousins, and E. A. Carlisle. 2012. "CO_2 Enrichment Inhibits Shoot Nitrate Assimilation in C_3 but Not C_4 Plants and Slows Growth Under Nitrate in C_3 Plants." *Ecology* 93, no. 2: 355–367.

Bloom, A. J., M. Burger, J. S. R. Asensio, and A. B. Cousins. 2010. "Carbon Dioxide Enrichment Inhibits Nitrate Assimilation in Wheat and *Arabidopsis*." *Science* 328: 899–903. https://doi.org/10.1126/science.1186440.

Bloom, A. J., and P. Kameritsch. 2017. "Relative Association of Rubisco With Manganese and Magnesium as a Regulatory Mechanism in Plants." *Physiologia Plantarum* 161, no. 4: 545–559. https://doi.org/10.1111/ppl.12616.

Bloom, A. J., P. Kasemsap, and J. S. Rubio-Asensio. 2020. "Rising Atmospheric CO_2 Concentration Inhibits Nitrate Assimilation in Shoots but Enhances it in Roots of C_3 Plants." *Physiologia Plantarum* 168, no. 4: 963–972. https://doi.org/10.1111/ppl.13040.

Bloom, A. J., and K. M. Lancaster. 2018. "Manganese Binding to Rubisco Could Drive a Photorespiratory Pathway That Increases the Energy Efficiency of Photosynthesis." *Nature Plants* 4: 414–422. https://doi.org/10.1038/s41477-018-0191-0.

Bloom, A. J., and R. E. Plant. 2021. "Wheat Grain Yield Decreased Over the Past 35 Years, But Protein Content Did Not Change." *Journal of Experimental Botany* 72, no. 20: 6811–6821. https://doi.org/10.1093/jxb/erab343.

Bloom, A. J., D. R. Smart, D. T. Nguyen, and P. S. Searles. 2002. "Nitrogen Assimilation and Growth of Wheat Under Elevated Carbon Dioxide." *Proceedings of the National Academy of Sciences* 99, no. 3: 1730–1735.

Bouvier, J. W., D. M. Emms, and S. Kelly. 2024. "Rubisco is Evolving for Improved Catalytic Efficiency and CO_2 Assimilation in Plants." *Proceedings of the National Academy of Sciences* 121, no. 11: e2321050121.

Budzianowska, A., and J. Budzianowski. 2022. "A New Flavonoid, a New Phenylethanoid Glycoside and Related Compounds Isolated From the Inflorescences of *Plantago Lanceolata* L." *Natural Product Research* 36, no. 15: 3813–3824.

Carlisle, E., S. Myers, V. Raboy, and A. Bloom. 2012. "The Effects of Inorganic Nitrogen Form and CO_2 Concentration on Wheat Yield and Nutrient Accumulation and Distribution." *Frontiers in Plant Science* 3: 195. https://doi.org/10.3389/fpls.2012.00195.

Christeller, J. T. 1981. "The Effects of Bivalent Cations on Ribulose Bisphosphate Carboxylase/Oxygenase." *Biochemical Journal* 193, no. 3: 839–844.

Christeller, J. T., and W. A. Laing. 1979. "Effects of Manganese Ions and Magnesium Ions on the Activity of Soya-Bean Ribulose Bisphosphate Carboxylase/Oxygenase." *Biochemical Journal* 183, no. 3: 747–750.

Cleland, W. W., T. J. Andrews, S. Gutteridge, F. C. Hartman, and G. H. Lorimer. 1998. "Mechanism of Rubisco: The Carbamate as General Base." *Chemical Reviews* 98, no. 2: 549–562. https://doi.org/10.1021/cr970010r.

Dietterich, L. H., A. Zanobetti, I. Kloog, et al. 2015. "Impacts of Elevated Atmospheric CO_2 on Nutrient Content of Important Food Crops." *Scientific Data* 2: 150036. https://doi.org/10.1038/sdata.2015.36.

Drava, G., L. Cornara, P. Giordani, and V. Minganti. 2019. "Trace Elements in *Plantago Lanceolata* L., a Plant Used for Herbal and Food Preparations: New Data and Literature Review." *Environmental Science and Pollution Research* 26: 2305–2313.

Easlon, H. M., and A. J. Bloom. 2013. "The Effects of Rising Atmospheric Carbon Dioxide on Shoot-Root Nitrogen and Water Signaling." *Frontiers in Plant Science* 4: 304. https://doi.org/10.3389/fpls.2013.00304.

Ellis, R. J. 1979. "The Most Abundant Protein in the World." *Trends in Biochemical Sciences* 4, no. 11: 241–244. https://doi.org/10.1016/0968-0004(79)90212-3.

Fischer, W. W., J. Hemp, and J. E. Johnson. 2016. "Evolution of Oxygenic Photosynthesis." *Annual Review of Earth and Planetary Sciences* 44: 647–683.

Fojtová, M., A. Kovařík, and R. Matyášek. 2001. "Cytosine Methylation of Plastid Genome in Higher Plants. Fact or Artefact." *Plant Science* 160, no. 4: 585–593.

Foyer, C. H., A. J. Bloom, G. Queval, and G. Noctor. 2009. "Photorespiratory Metabolism: Genes, Mutants, Energetics, and Redox Signaling." *Annual review of plant biology* 60: 455–484.

Gonçalves, S., and A. Romano. 2016. "The Medicinal Potential of Plants from the Genus *Plantago* (Plantaginaceae)." *Industrial Crops and Products* 83: 213–226.

Guarrera, P. M., and V. Savo. 2016. "Wild Food Plants Used in Traditional Vegetable Mixtures in Italy." *Journal of Ethnopharmacology* 185: 202–234.

Hagège, A., T. N. S. Huynh, and M. Hébrant. 2015. "Separative Techniques for Metalloproteomics Require Balance Between Separation and Perturbation." *TrAC, Trends in Analytical Chemistry* 64: 64–74. https://doi.org/10.1016/j.trac.2014.08.013.

Hagemann, M., R. Kern, V. G. Maurino, et al. 2016. "Evolution of Photorespiration From Cyanobacteria to Land Plants, Considering Protein Phylogenies and Acquisition of Carbon Concentrating Mechanisms." *Journal of Experimental Botany* 67, no. 10: 2963–2976. https://doi.org/10.1093/jxb/erw063.

Houtz, R. L., R. Magnani, N. R. Nayak, and L. M. A. Dirk. 2007. "Co- And Post-Translational Modifications in Rubisco: Unanswered Questions." *Journal of Experimental Botany* 59, no. 7: 1635–1645.

Iñiguez, C., Ü. Niinemets, K. Mark, and J. Galmés. 2021. "Analyzing the Causes of Method-To-Method Variability Among Rubisco Kinetic Traits: From the First to the Current Measurements." *Journal of Experimental Botany* 72, no. 22: 7846–7862. https://doi.org/10.1093/jxb/erab356.

J. Bloom, A., M. Burger, B. A. Kimball, and P. J. Pinter. 2014. "Nitrate Assimilation Is Inhibited by Elevated CO_2 in Field-Grown Wheat." *Nature Climate Change* 4: 477–480. https://doi.org/10.1038/nclimate2183.

Jordan, D. B., and W. L. Ogren. 1983. "Species Variation in Kinetic Properties of Ribulose 1, 5-bisphosphate Carboxylase/Oxygenase." *Archives of Biochemistry and Biophysics* 227, no. 2: 425–433.

Kapralov, M. V., and D. A. Filatov. 2007. "Widespread Positive Selection in the Photosynthetic Rubisco Enzyme." *BMC Evolutionary Biology* 7: 73.

Karkehabadi, S., T. C. Taylor, and I. Andersson. 2003. "Calcium Supports Loop Closure but Not Catalysis in Rubisco." *Journal of Molecular Biology* 334, no. 1: 65–73.

Knight, S., I. Andersson, and C.-I. Brändén. 1990. "Crystallographic Analysis of Ribulose 1,5-bisphosphate Carboxylase From Spinach at 2·4 Å Resolution." *Journal of Molecular Biology* 215, no. 1: 113–160.

Langdale, J. A., W. C. Taylor, and T. Nelson. 1991. "Cell-Specific Accumulation of Maize Phosphoenolpyruvate Carboxylase Is Correlated With Demethylation at a Specific Site 3 Kb Upstream of the Gene." *Molecular and General Genetics MGG* 225: 49–55.

Lingappa, U. F., D. R. Monteverde, J. S. Magyar, J. S. Valentine, and W. W. Fischer. 2019. "How Manganese Empowered Life With Dioxygen (And Vice Versa)." *Free Radical Biology and Medicine* 140: 113–125. https://doi.org/10.1016/j.freeradbiomed.2019.01.036.

van Lun, M., J. S. Hub, D. van der Spoel, and I. Andersson. 2014. "CO_2 and O_2 Distribution in Rubisco Suggests the Small Subunit Functions as a CO_2 Reservoir." *Journal of the American Chemical Society* 136, no. 8: 3165–3171.

Mao, Y., E. Catherall, A. Díaz-Ramos, et al. 2023. "The Small Subunit of Rubisco and Its Potential as an Engineering Target." *Journal of Experimental Botany* 74, no. 2: 543–561. https://doi.org/10.1093/jxb/erac309.

Marano, M. R., and N. Carrillo. 1991. "Chromoplast Formation During Tomato Fruit Ripening. No Evidence for Plastid DNA Methylation." *Plant Molecular Biology* 16: 11–19.

Martin, M. N., and F. R. Tabita. 1981. "Differences in the Kinetic Properties of the Carboxylase and Oxygenase Activities of Ribulose Bisphosphate Carboxylase/Oxygenase." *FEBS Letters* 129, no. 1: 39–43.

Miszalski, Z., P. Kaszycki, M. Śliwa-Cebula, et al. 2023. "Plasticity of *Plantago Lanceolata* L. in Adaptation to Extreme Environmental Conditions." *International Journal of Molecular Sciences* 24, no. 17: 13605.

Montes-Bayón, M., E. Blanco-González, and B. Michalke. 2016. "Metalloproteins." In *Metallomics*, edited by B. Michalke, 357. Weinheim, Germany: Wiley-VCH Verlag GmbH & Co. KGaA.

Murai, M., Y. Tamayama, and S. Nishibe. 1995. "Phenylethanoids in the Herb of *Plantago Lanceolata* and Inhibitory Effect on Arachidonic Acid-Induced Mouse Ear Edema." *Planta Medica* 61, no. 05: 479–480.

Myers, S. S., A. Zanobetti, I. Kloog, et al. 2014. "Increasing CO_2 Threatens Human Nutrition." *Nature* 510, no. 7503: 139–142. https://doi.org/10.1038/nature13179.

Ngernprasirtsiri, J., H. Kobayashi, and T. Akazawa. 1988. "DNA Methylation as a Mechanism of Transcriptional Regulation in Non-photosynthetic Plastids in Plant Cells." *Proceedings of the National Academy of Sciences* 85, no. 13: 4750–4754.

Ohta, N., N. Sato, S. Kawano, and T. Kuroiwa. 1991. "Methylation of DNA in the Chloroplasts and Amyloplasts of the Pea, *Pisum Sativum*." *Plant Science* 78, no. 1: 33–42.

Rachmilevitch, S., A. B. Cousins, and A. J. Bloom. 2004. "Nitrate Assimilation in Plant Shoots Depends on Photorespiration." *Proceedings of the National Academy of Sciences* 101, no. 31: 11506–11510.

Rahamouz-Haghighi, S., K. Bagheri, N. Mohsen-Pour, and A. Sharafi. 2022. "In Vitro Evaluation of Cytotoxicity and Antibacterial Activities of Ribwort Plantain (*Plantago Lanceolata* L.) Root Fractions and Phytochemical Analysis by Gas Chromatography-Mass Spectrometry." *Archives of Razi Institute* 77, no. 6: 2131–2143.

Raverdy, S., Y. Zhang, J. Foster, and C. K. S. Carlow. 2007. "Molecular and Biochemical Characterization of Nematode Cofactor Independent Phosphoglycerate Mutases." *Molecular and Biochemical Parasitology* 156, no. 2: 210–216.

Rubio-Asensio, J. S., and A. J. Bloom. 2017. "Inorganic Nitrogen Form: A Major Player in Wheat and *Arabidopsis* Responses to Elevated Co_2." *Journal of Experimental Botany* 68, no. 10: 2611–2625. https://doi.org/10.1093/jxb/erw465.

Saban, J. M., M. A. Chapman, and G. Taylor. 2019. "Face Facts Hold for Multiple Generations; Evidence from Natural Co_2 Springs." *Global Change Biology* 25, no. 1: 1–11.

Saban, J. M., A. Watson-Lazowski, M. A. Chapman, and G. Taylor. 2020. "The Methylome is Altered for Plants in a High CO_2 World: Insights into the Response of a Wild Plant Population to Multigenerational Exposure to Elevated Atmospheric [CO_2]." *Global Change Biology* 26, no. 11: 6474–6492.

Segura-Broncano, L., K. R. Pukacz, V. Reichel-Deland, U. Schlüter, S. Triesch, and A. P. M. Weber. 2023. "Photorespiration Is the Solution, Not the Problem." *Journal of Plant Physiology* 282: 153928. https://doi.org/10.1016/j.jplph.2023.153928.

Shi, C., N. Hu, H. Huang, J. Gao, Y.-J. Zhao, and L.-Z. Gao. 2012. "An Improved Chloroplast DNA Extraction Procedure for Whole Plastid Genome Sequencing." *PLoS One* 7, no. 2: e31468.

Shi, X., and A. Bloom. 2021. "Photorespiration: The Futile Cycle?" *Plants* 10, no. 5: 908.

Shi, X., N. M. Hannon, and A. J. Bloom. 2024. "Metals and Other Ligands Balance Carbon Fixation and Photorespiration in Chloroplasts." *Physiologia Plantarum* 176, no. 4: e14463. https://doi.org/10.1111/ppl.14463.

Smart, D. R., and A. J. Bloom. 2001. "Wheat Leaves Emit Nitrous Oxide During Nitrate Assimilation." *Proceedings of the National Academy of Sciences* 98, no. 14: 7875–7878.

Smart, D. R., K. Ritchie, A. J. Bloom, and B. B. Bugbee. 1998. "Nitrogen Balance for Wheat Canopies (Triticum Aestivumcv. Veery 10) Grown Under Elevated and Ambient Co2concentrations." *Plant, Cell & Environment* 21, no. 8: 753–763.

Smith, K., D. D. Strand, D. M. Kramer, and B. J. Walker. 2024. "The Role of Photorespiration in Preventing Feedback Regulation via Atp Synthase in *Nicotiana Tabacum*." *Plant, Cell & Environment* 47, no. 2: 416–428.

South, P. F., A. P. Cavanagh, H. W. Liu, and D. R. Ort. 2019. "Synthetic Glycolate Metabolism Pathways Stimulate Crop Growth and Productivity in the Field." *Science* 363, no. 6422: eaat9077.

Spreitzer, R. J. 2003. "Role of the Small Subunit in Ribulose-1, 5-Bisphosphate Carboxylase/Oxygenase." *Archives of Biochemistry and Biophysics* 414, no. 2: 141–149.

Taylor, T. C., and I. Andersson. 1997. "The Structure of the Complex between Rubisco and Its Natural Substrate Ribulose 1, 5-Bisphosphate." *Journal of Molecular Biology* 265, no. 4: 432–444.

Tienderen, P. H. V., and J. van der Toorn. 1991. "Genetic Differentiation between Populations of *Plantago Lanceolata*. I. Local Adaptation in Three Contrasting Habitats." *The Journal of Ecology* 79: 27–42.

Watson-Lazowski, A., Y. Lin, F. Miglietta, R. J. Edwards, M. A. Chapman, and G. Taylor. 2016. "Plant Adaptation or Acclimation to Rising CO_2? Insight From First Multigenerational RNA-Seq Transcriptome." *Global Change Biology* 22, no. 11: 3760–3773.

Whitney, S. M., R. E. Sharwood, D. Orr, S. J. White, H. Alonso, and J. Galmés. 2011. "Isoleucine 309 Acts as a C_4 Catalytic Switch That Increases ribulose-1,5-Bisphosphate Carboxylase/Oxygenase (Rubisco) Carboxylation Rate in *Flaveria*." *Proceedings of the National Academy of Sciences* 108, no. 35: 14688–14693. https://doi.org/10.1073/pnas.1109503108.

Wichtl, M. 2004. *Herbal Drugs and Phytopharmaceuticals: A Handbook for Practice on a Scientific Basis*. CRC press.

Wildner, G. F., and J. Henkel. 1979. "The Effect of Divalent Metal Ions on the Activity of Mg^{++} Depleted ribulose-1, 5-bisphosphate Oxygenase." *Planta* 146, no. 2: 223–228.

Wingfield, P. 1998. "Protein Precipitation Using Ammonium Sulfate." *Current Protocols in Protein Science* 13: A.3F.1–A.3F.8.

Yamada, K., I. I. Davydov, G. Besnard, and N. Salamin. 2019. "Duplication History and Molecular Evolution of the *Rbcs* Multigene Family in Angiosperms." *Journal of Experimental Botany* 70, no. 21: 6127–6139.

Yoshida, T., K. Rikimaru, M. Sakai, S. Nishibe, T. Fujikawa, and Y. Tamura. 2013. "*Plantago lanceolata* L. Leaves Prevent Obesity in C57BL/6 J Mice Fed a High-Fat Diet." *Natural Product Research* 27, no. 11: 982–987.

Zhang, Y., J. M. Foster, S. Kumar, M. Fougere, and C. K. S. Carlow. 2004. "Cofactor-Independent Phosphoglycerate Mutase Has an Essential Role in *Caenorhabditis Elegans* and Is Conserved in Parasitic Nematodes." *Journal of Biological Chemistry* 279, no. 35: 37185–37190.

Zhao, F., B. Liu, S. Liu, et al. 2023. "Disentangling a 40-year-old Taxonomic Puzzle: The Phylogenetic Position of *Mimulicalyx* (Lamiales)." *Botanical Journal of the Linnean Society* 201, no. 2: 135–153.

Supporting Information

Additional supporting information can be found online in the Supporting Information section.